

Images of black holes viewed by distant observer

Vyacheslav Ivanovich Dokuchaev^{1,2,*}

¹*Institute for Nuclear Research of the Russian Academy of Sciences 60th October Anniversary Prospect 7a, 117312 Moscow, Russia*

²*Moscow Institute of Physics and Technology, 9 Institutskiy per., Dolgoprudny, 141701 Moscow Region Russia*

(Dated: January 4, 2024)

Possible forms of black hole images, viewed by a distant observer, are calculated basing on general relativity and equations of motion in the Kerr-Newman metric. Black hole image is a gravitationally lensed image of the black hole event horizon. It may be viewed as a black spot on the celestial sphere, projected inside the position of classical black hole shadow. In the nearest future it would be possible to verify modified gravity theories by observations of astrophysical black hole with Space Observatory Millimetron.

PACS numbers: 04.20.Fy, 04.20.Jb, 04.50.Kd, 04.60.Bc, 04.70.Bw

I. INTRODUCTION

How black hole looks like? It is a standard question of both scientific experts and men in the streets. In this paper the black hole images are calculated basing on general relativity and equations of motion in the classical Kerr–Newman metric [1–6], describing the rotating and electrically charged black hole (see Appendix A, B and C for details). These images are the gravitationally lensed images of black hole event horizon.

Numerical supercomputer simulations of general relativistic hydro-magnetic accretion onto black (see, e. g., [7–13]) affirm the Blandford-Znajek mechanism [14] of energy extraction from fast rotating Kerr black holes. The crucial

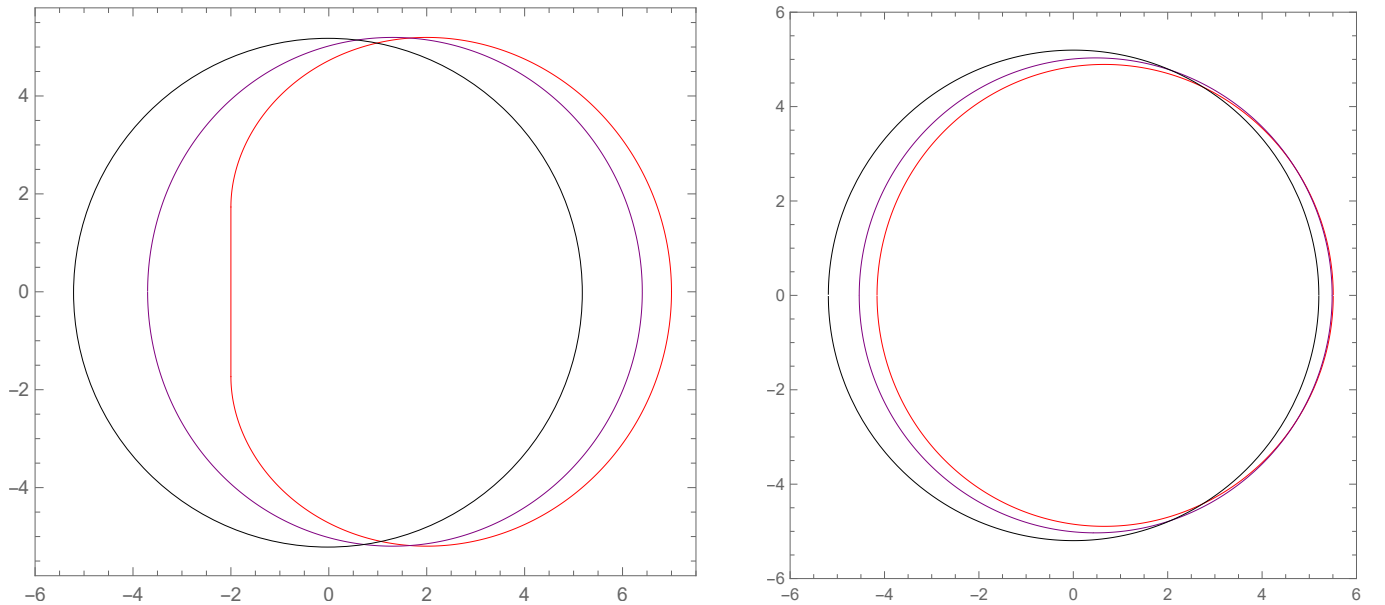


FIG. 1. Some examples of classical black hole shadows are shown for the cases of supermassive black holes SgrA* and M87*. Left panel: the shadows of SgrA* (with a possible inclinations of rotation axes with respect to the polar angle θ_0) in the spherically symmetric Schwarzschild case ($a = 0$) is black circle with a radius $r_{\text{sh}} = 3\sqrt{3} \approx 5.196$. The closed red curve is the shadow of extremely fast rotating black hole ($a = 1$) and closed purple curve ($a = 0.65$), respectively. Note, that the vertical sizes of shadows in the case of SgrA* are independent on the values of spin a . Right pane: The corresponding forms of shadows in the case of M87* (with a possible inclinations of rotation axes with respect to the polar angle $\theta_0 = 163^\circ$) for spin values $a = 1$ (red closed curve), $a = 0.75$ (purple closed curve), and $a = 0$ (black circle) of radius $r_{\text{sh}} = 3\sqrt{3}$.

* e-mail: dokuchaev@inr.ac.ru

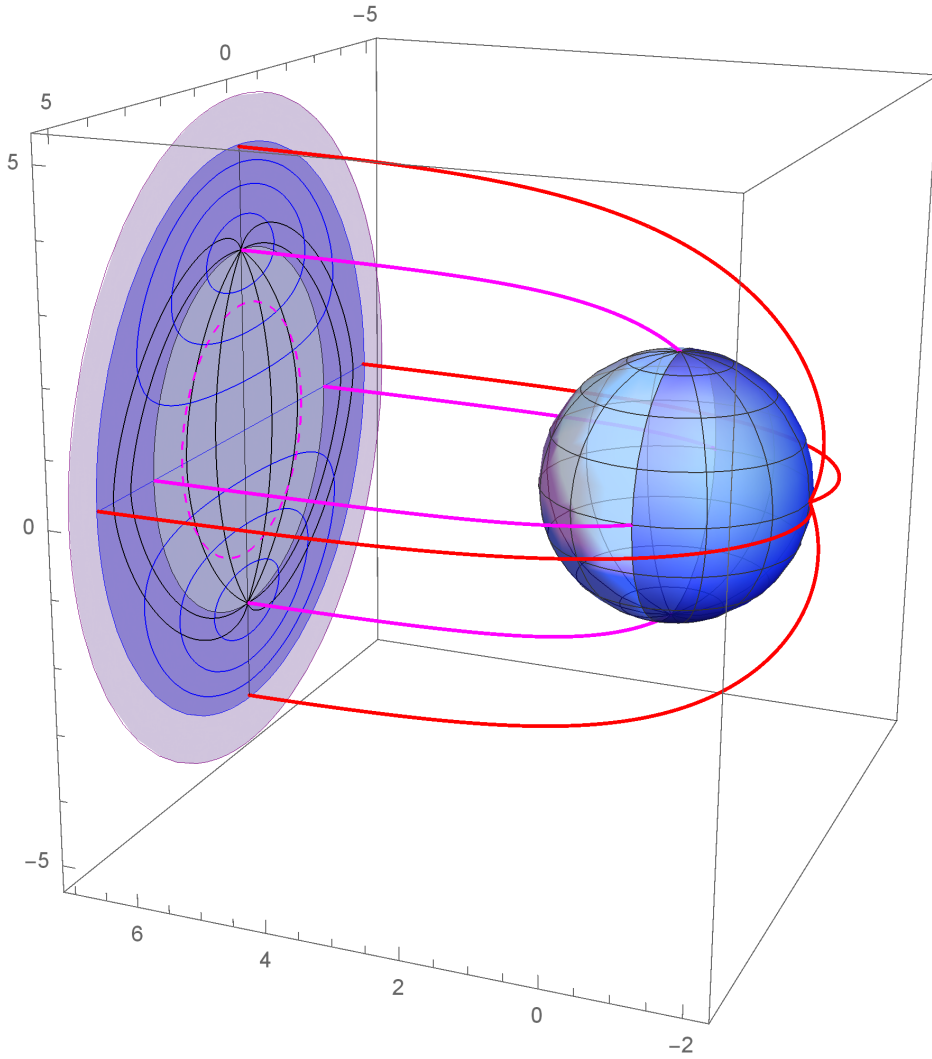


FIG. 2. Reconstruction of the Schwarzschild black hole event horizon silhouette using 3D trajectories of photons (multicolored curves), which start very near the black hole event horizon and are registered by a distant observer (by a distant telescope). The event horizon silhouette always projects at the celestial sphere within the classical black hole shadow with a radius $3\sqrt{3}$. Meanwhile, the corresponding radius of event horizon silhouette is $r_h \approx 4.457$ [15, 16].

feature of this mechanism is an electric current flowing through the black hole immersed into external poloidal magnetic field. This electric current heats the accreting plasma up to the nearest outskirts of the black hole event horizon. Very high luminosity of this hot accreting plasma will spoil some parts of the black spots at the astrophysical black hole images.

Images of astrophysical black holes may be viewed as black spots on the celestial sphere, projected inside the possible positions of classical black hole shadows. See at Fig. 1 some examples of the classical black hole shadows.

It must be stressed that the forms of discussed dark spots are independent on the distribution and emission of the accreting plasma. Instead of, the corresponding forms of dark spots are completely defined by the properties of black hole gravitational field and black hole parameters like black hole mass M and spin a . (Throughout this paper we use the standard dimensionless units with $GM/c^2 = 1$, where G — newtonian gravitational constant, c — velocity of light).

See at Fig. 2 the example of reconstruction of the spherically symmetric Schwarzschild black hole event horizon silhouette using 3D trajectories of photons (multicolored curves), which start very near the black hole event horizon and are registered by a distant observer (by a distant telescope). Correspondingly, at Fig. 3 is shown the example of reconstruction of the extremely fast rotating Kerr black hole with spin $a = 1$.

The trajectories of photons at all Figures of this paper are calculated numerically by using test particle equations of motion in the Kerr metric (see Appendix B and C). The event horizon silhouette (dark spot) always projects at the

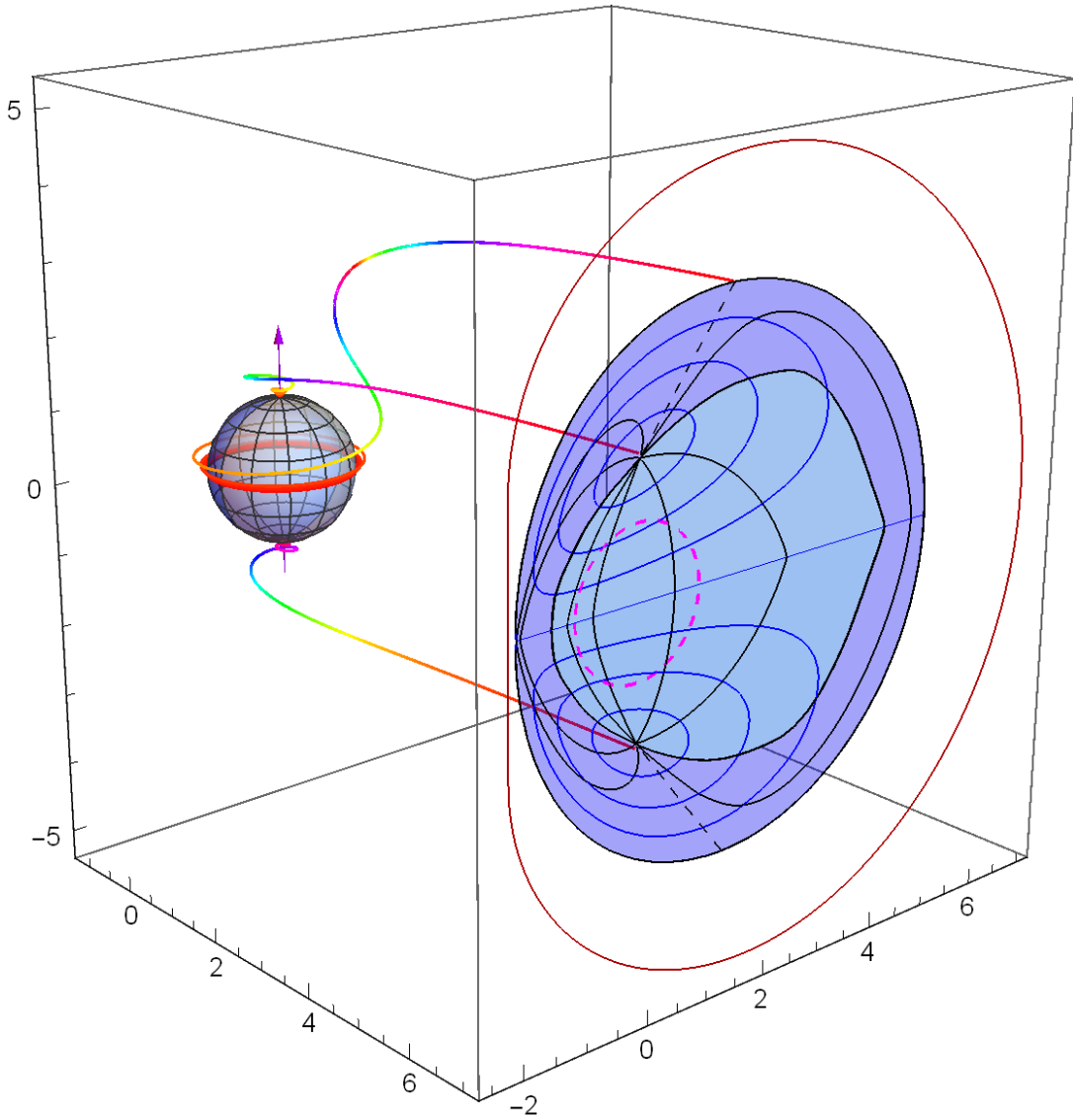


FIG. 3. Reconstruction of extremely fast Kerr black hole ($a = 1$) event horizon silhouette for the rotation axes orientation of the supermassive black hole SgrA*. It is used 3D trajectories of photons (multicolored curves), which start very near the black hole event horizon and are registered by a distant observer (by a distant telescope). The nearest hemisphere of the event horizon is projected into (light blue) disk with radius $r_{EW} \simeq 2.848$. The farthest hemisphere is projected into the hollow (dark blue) disk with radius $r_{eh} \simeq 4.457$. It is a radius of the gravitationally lensed event horizon image. The blue and black curves are the corresponding parallels and meridians at the event horizon globe.

celestial sphere within the classical black hole shadow.

II. CLASSICAL BLACK HOLE SHADOW

The apparent shape of the black hole shadow, as seen by a distant observer in the equatorial plane, is determined parametrically, $(\lambda, q) = (\lambda(r), q(r))$, from simultaneous solution of equations $V_r(r) = 0$ and $[rV_r(r)]' = 0$ (see e. g.,

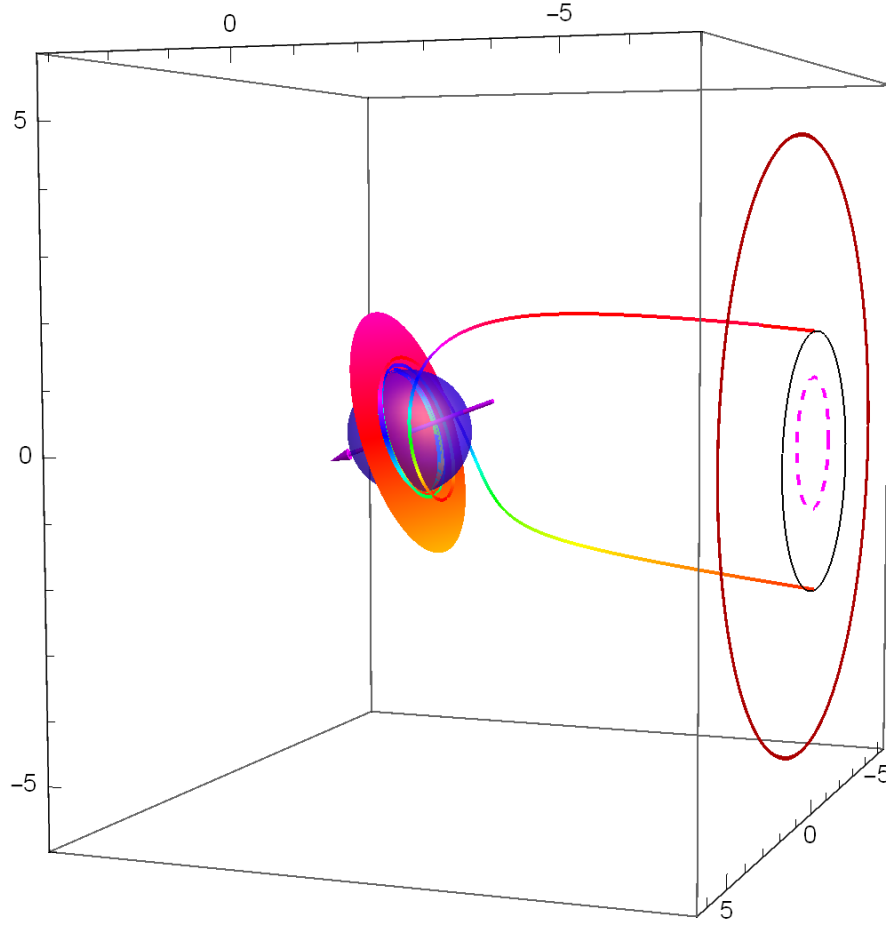


FIG. 4. A 3D picture of the supermassive black hole with spin parameter $a = 1$ surrounded by thin accretion disk. A 17° inclination angle of M87* rotation axis with respect to a distant observer is supposed.

[6, 17, 18]):

$$\lambda = \frac{-r^3 + 3r^2 - a^2(r+1)}{a(r-1)}, \quad (1)$$

$$q^2 = \frac{r^3[4a^2 - r(r-3)^2]}{a^2(r-1)^2}. \quad (2)$$

Some examples of the classical black hole shadows are shown at Fig. 1 for the cases of supermassive black holes M87* at the center of galaxy M87 and SgrA* at the center of our native Milky Way galaxy. Left panel: the shadows of SgrA* (with a possible inclinations of rotation axes with respect to the polar angle θ_0) in the spherically symmetric Schwarzschild case ($a = 0$) is black circle with a radius $r_{\text{sh}} = 3\sqrt{3} \approx 5.196$. The closed red curve is the shadow of extremely fast rotating black hole ($a = 1$) and closed purple curve ($a = 0.65$), respectively. Note, that the vertical sizes of shadows in the case of SgrA* are independent on the values of spin a . Right pane: The corresponding forms of shadows in the case of M87* (with a possible inclinations of rotation axes with respect to the polar angle $\theta_0 = 163^\circ$) for spin values $a = 1$ (red closed curve), $a = 0.75$ (purple closed curve), and $a = 0$ (black circle) of radius $r_{\text{sh}} = 3\sqrt{3}$.

See at Fig. 7 the numerical simulation of compact spherical probe (neutron star or spaceship) orbiting around a fast rotating black hole ($a = 0.9982$) at a circular orbit with a dimensionless radius $r = 20$. It is shown one orbital period in discrete time intervals. A distant observer is placed a little bit above the black hole equatorial plane. It is shown the direct image and also the first and the second light echoes. The gray region is the classical black hole shadow. The images second light echo is concentrated at the outskirts of the shadow. It is also taken into account the gravitational lensing of spherical probe in the black hole gravitational field (in the ellipsoidal approximation), viewed by distant observer as deformation of the probe. For details see [35, 36].

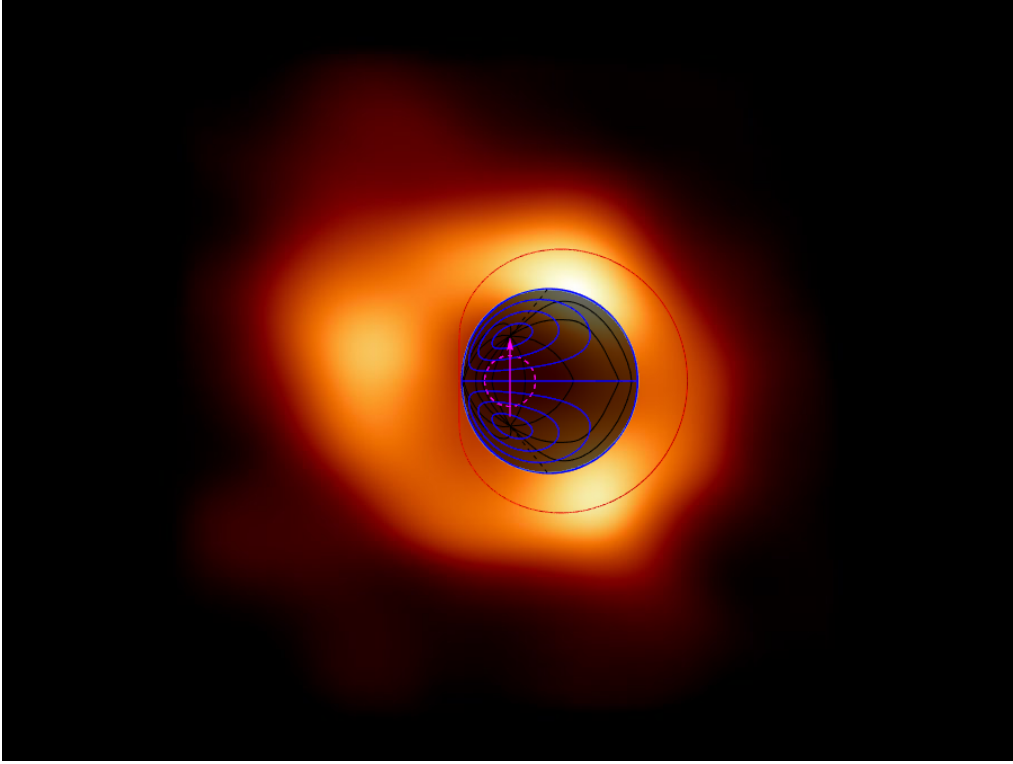


FIG. 5. A composition of the Event Horizon Telescope image of supermassive black hole SgrA* [21–27] with the numerically modeled dark spot, corresponding to the gravitationally lensed image of the event horizon globe with spin $a = 1$. The closed purple curve is the outline of classical black hole shadow. The magenta arrow is the direction of black hole rotation axis. The magenta dashed circle is a position of the black hole event horizon with radius $r_h = 1$ in the Euclidean space without gravity.

III. DARK SPOTS AT BLACK HOLE IMAGES

The form of a dark spot at the astrophysical black hole image, which is viewed by a distant telescope (observer) at the black hole equatorial plane may be calculated by using Brandon Carter [4] integral equation of motion in the Kerr metric

$$\int_2^\infty \frac{dr}{\sqrt{V_r}} = 2 \int_{\theta_{\min}}^{\pi/2} \frac{d\theta}{\sqrt{V_\theta}}. \quad (3)$$

where θ_{\min} is a turning point of the photon trajectory for direct image in the polar direction (for details, see [19, 20]).

In the Schwarzschild case a turning point is at polar angle $\theta_{\min} = \arccos(q/\sqrt{q^2 + \lambda^2})$, where q and λ are parameters of photon trajectories from equation (A8). Respectively, from the right-hand-side integral in (3) is $\pi/\sqrt{q^2 + \lambda^2}$. The resulting numerical solution of integral equation (3) provides the radius of event horizon image $r_{\text{eh}} = \sqrt{q^2 + \lambda^2} = 4.457$. The nearest hemisphere of the event horizon is projected into (light blue) disk with radius $r_{\text{EW}} \simeq 2.848$. The farthest hemisphere is projected into the hollow (dark blue) disk with radius $r_{\text{eh}} \simeq 4.457$. It is a radius of the gravitationally lensed event horizon image. At Fig. 2 and 3 are shown the corresponding numerical solutions for the gravitationally lensed event horizon images in the Schwarzschild ($a = 0$) and extremely fast Kerr rotation case ($a = 1$) for the rotation axes orientation of the supermassive black hole SgrA*. The near hemisphere of the event horizon is projected by the lensing photons into the central (dark blue) region. Respectively the far hemisphere is projected into the hollow (light blue) region. The blue and black curves are the corresponding parallels and meridians at the event horizon globe.

The event horizon globe of the Kerr black hole ($e = 0, a \neq 0$) according to general equation (A5) is rotating with an angular velocity as a solid body

$$\Omega_h = \frac{a}{2(1 + \sqrt{1 - a^2})}. \quad (4)$$

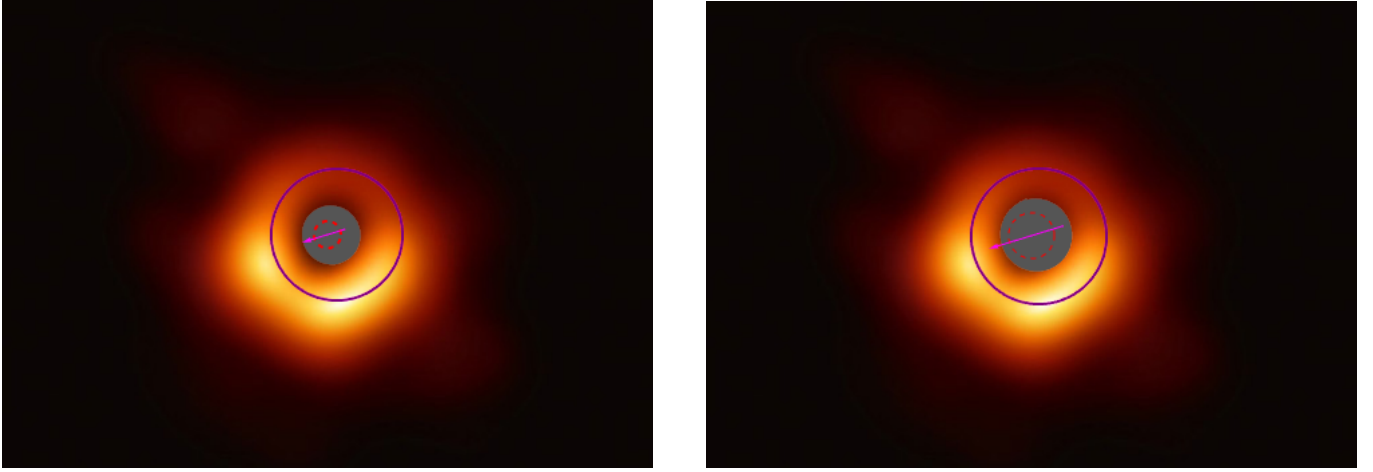


FIG. 6. Superposition of the modeled dark spot with the Event Horizon Telescope image of supermassive black hole M87*: Left panel, $a = 1$; right panel, $a = 0.75$. A 17° inclination angle of the black hole rotation axis at the celestial sphere is supposed. Note that the size of dark spot in the case of rotation axis orientation of this black hole is weakly depends on the value of spin parameter a .

See at Fig. 8 the gravitationally lensed images in discrete time intervals of small probe (neutron star or cosmic ship) with a zero angular momentum ($\lambda = 0$) and zero Carter constant ($q = 0$), which is plunging into a fast rotating black hole. A distant observer is placed a little bit above the black hole equatorial plane. The small probe is winding around the black hole equator of the event horizon globe. It is shown one circle of this winding. The escaping signals from this prob are exponentially fading in time. For numerical animation see [37].

IV. DISCUSSIONS AND CONCLUSIONS

In this paper the possible forms of black hole images, viewed by a distant observer, are calculated basing on general relativity and equations of motion in the Kerr-Newman metric. Black hole image is a gravitationally lensed image of the black hole event horizon. It may be viewed as a black spot on the celestial sphere, projected inside the position of classical black hole shadow. The event horizon silhouette (dark spot) always projects at the celestial sphere within the classical black hole shadow.

Images of astrophysical black holes may be viewed as black spots on the celestial sphere, projected inside the possible positions of classical black hole shadows. Very high luminosity of hot accreting plasma will spoil some parts of the black spots at the astrophysical black hole images.

It must be stressed that the forms of discussed dark spots are independent on the distribution and emission of the accreting plasma. Instead of, the corresponding forms of dark spots are completely defined by the properties of black hole gravitational field and black hole parameters like black hole mass M and spin a .

In the nearest future it would be possible to verify modified gravity theories by observations of astrophysical black hole with international Millimetron Space Observatory [40–43].

ACKNOWLEDGMENTS

Author is grateful to E. O. Babichev, V. A. Berezin, Yu. N. Eroshenko, N. O. Nazarova and A. L. Smirnov for stimulating discussions.

Appendix A: Kerr–Newman metric

The line element of the classical Kerr–Newman metric [1–6], describing in particular the rotating ($a \neq 0$) and electrically charged ($e \neq 0$) black hole, is

$$ds^2 = -e^{2\nu} dt^2 + e^{2\psi} (d\phi - \omega dt)^2 + e^{2\mu_1} dr^2 + e^{2\mu_2} d\theta^2, \quad (\text{A1})$$

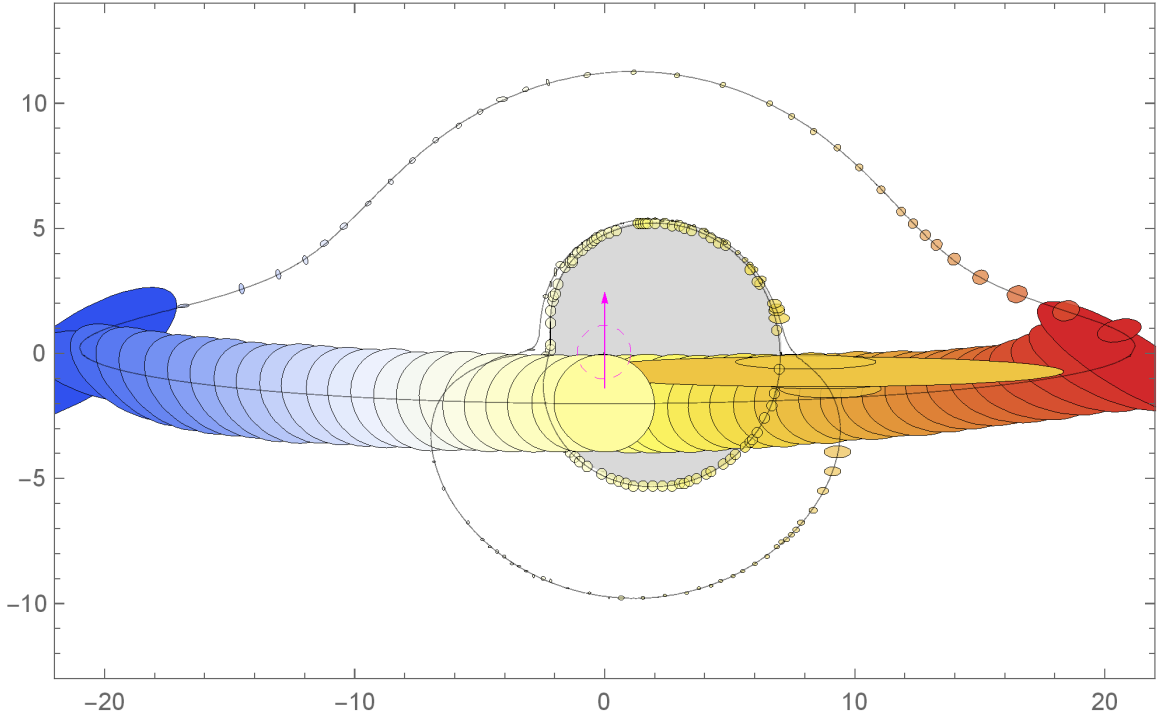


FIG. 7. The numerical simulation of compact spherical probe (neutron star or spaceship) orbiting around a fast rotating black hole ($a = 0.9982$) at a circular orbit with a dimensionless radius $r = 20$. It is shown one orbital period in discrete time intervals. A distant observer is placed a little bit above the black hole equatorial plane. It is shown the direct image and also the first and the second light echoes. The gray region is the classical black hole shadow. The images second light echo is concentrated at the outskirts of the shadow. It is also taken into account the gravitational lensing of spherical probe in the black hole gravitational field (in the ellipsoidal approximation), viewed by distant observer as deformation of the probe. For details see [35, 36].

where

$$e^{2\nu} = \frac{\Sigma\Delta}{A}, \quad e^{2\psi} = \frac{A \sin^2 \theta}{\Sigma}, \quad e^{2\mu_1} = \frac{\Sigma}{\Delta}, \quad e^{2\mu_2} = \Sigma, \quad \omega = \frac{2Mar}{A}, \quad (\text{A2})$$

$$\Delta = r^2 - 2Mr + a^2 + e^2, \quad \Sigma = r^2 + a^2 \cos^2 \theta, \quad A = (r^2 + a^2)^2 - a^2 \Delta \sin^2 \theta, \quad (\text{A3})$$

where M is black hole mass, $a = J/M$ is black hole specific angular momentum (spin), e is black hole electric charge, ω is frame-dragging angular velocity.

Roots of equation $\Delta = 0$ define the black hole event horizon radius r_+ and the Cauchy radius r_- :

$$r_{\pm} = 1 \pm \sqrt{1 - a^2 - q^2}. \quad (\text{A4})$$

The event horizon of the Kerr-Newman black hole rotates as a solid body with (i. e., independent of the polar angle θ) with angular velocity

$$\omega_+ = \frac{2Mar_+}{(r_+^2 + a^2)^2} \quad (\text{A5})$$

According to Brandon Carter equations of motion [4] there are the following integrals of motion: μ is particle mass, E is particle total energy, L is particle azimuth angular momentum and Q is the specific Carter constant, defining the non-equatorial motion. The corresponding radial potential $R(r)$ is

$$R(r) = P^2 - \Delta[\mu^2 r^2 + (L - aE)^2 + Q], \quad (\text{A6})$$

where $P = E(r^2 + a^2) - aL$. The polar potential $\Theta(\theta)$ is

$$\Theta(\theta) = Q - \cos^2 \theta [a^2(\mu^2 - E^2) + L^2 \sin^{-2} \theta]. \quad (\text{A7})$$

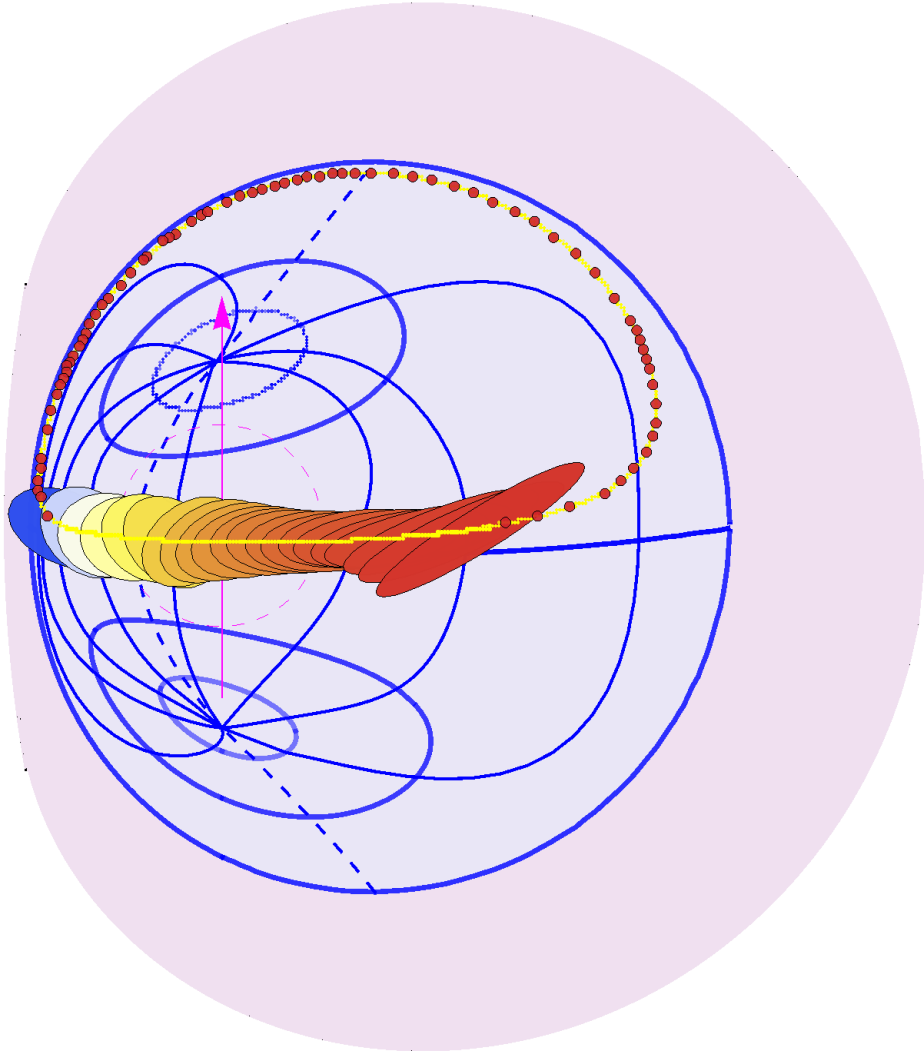


FIG. 8. Gravitationally lensed images in discrete time intervals of small probe (neutron star or cosmic ship) with a zero angular momentum ($\lambda = 0$) and zero Carter constant ($q = 0$), which is plunging into a fast rotating black hole. A distant observer is placed a little bit above the black hole equatorial plane. The small probe is winding around the black hole equator of the event horizon globe. It is shown one circle of this winding. The escaping signals from this prob are exponentially fading in time. For numerical animation see [37].

Particle trajectories depend on three parameters

$$\gamma = \frac{E}{\mu}, \quad \lambda = \frac{L}{\mu}, \quad q = \frac{\sqrt{Q}}{E}. \quad (\text{A8})$$

For massless particles like photons there are two parameters: λ and q . The corresponding horizontal and vertical impact parameters, α and β , which are viewed on the celestial sphere by a distant observer, placed at the polar angle θ_0 are [17, 19, 20]):

$$\alpha = -\frac{\lambda}{\sin \theta_0}, \quad \beta = \pm \sqrt{\Theta(\theta_0)}. \quad (\text{A9})$$

From astrophysical point of view (see, e. g., [32–34]) the most probable are the cases of fast-rotating supermassive black holes with spin values close to the maximum value, $a_{\max} = 1$.

Appendix B: Equations of motion for test particles

The first order differential equations of motion in the Kerr-Newman metric, derived by Brandon Carter [4], are

$$\Sigma \frac{dr}{d\tau} = \pm \sqrt{R(r)}, \quad (\text{B1})$$

$$\Sigma \frac{d\theta}{d\tau} = \pm \sqrt{\Theta(\theta)}, \quad (\text{B2})$$

$$\Sigma \frac{d\phi}{d\tau} = L \sin^{-2} \theta + a(\Delta^{-1}P - E), \quad (\text{B3})$$

$$\Sigma \frac{dt}{d\tau} = a(L - aE \sin^2 \theta) + (r^2 + a^2)\Delta^{-1}P, \quad (\text{B4})$$

where τ — a proper time of the massive ($\mu \neq 0$) particle or an affine parameter of massless ($\mu = 0$) particle like photons.

Appendix C: Integral equations for test particle motion

For numerical calculations are very useful the integral equations of motion (B1)–(B4):

$$\int \frac{dr}{\sqrt{R(r)}} = \int \frac{d\theta}{\sqrt{\Theta(\theta)}}, \quad (\text{C1})$$

$$\tau = \int \frac{r^2}{\sqrt{R(r)}} dr + \int \frac{a^2 \cos^2 \theta}{\sqrt{\Theta(\theta)}} d\theta, \quad (\text{C2})$$

$$\phi = \int \frac{aP}{\Delta \sqrt{R(r)}} dr + \int \frac{L - aE \sin^2 \theta}{\sin^2 \theta \sqrt{\Theta(\theta)}} d\theta, \quad (\text{C3})$$

$$t = \int \frac{(r^2 + a^2)P}{\Delta \sqrt{R(r)}} dr + \int \frac{(L - aE \sin^2 \theta)a}{\sqrt{\Theta(\theta)}} d\theta. \quad (\text{C4})$$

The integrals in equations (C1)–(C4) monotonically grow along the particle trajectory and change sign at both the radial and polar turning points:

$$\int_{r_0}^{r_s} \frac{dr}{\sqrt{R(r)}} = \int_{\theta_0}^{\theta_s} \frac{d\theta}{\sqrt{\Theta(\theta)}}, \quad (\text{C5})$$

where r_s and θ_s are, respectively the initial and polar particle coordinates, and $r_0 \gg r_h$ and θ_0 are the corresponding final particle coordinates. The more complicated case is with the one turning point in the latitude (or polar) direction, $\theta_{\min}(\lambda, q)$, which is a solution of the equation $\Theta(\theta) = 0$. The corresponding ordinary integrals in equation (C1) are written as

$$\int_{r_s}^{r_0} \frac{dr}{\sqrt{R(r)}} = \int_{\theta_{\min}}^{\theta_s} \frac{d\theta}{\sqrt{\Theta(\theta)}} + \int_{\theta_{\min}}^{\theta_0} \frac{d\theta}{\sqrt{\Theta(\theta)}}. \quad (\text{C6})$$

We use these equations in our numerical calculations of photon trajectories, starting in the vicinity of Kerr-Newman black hole and finishing at the position of a distant observer very far from black hole.

[1] Kerr, R.P. Gravitational Field of a Spinning Mass as an Example of Algebraically Special Metrics. *Phys. Rev. Lett.* **1963**, *11*, 237–238.

- [2] Newman, E.; Janis, A. Note on the Kerr Spinning-Particle Metric. *Commun. in Math. Phys.* **1965**, *6*, 915–917.
- [3] Newman, E.; Couch, E.; Chinnapared, K.; Exton, A.; Prakash, A.; Torrence, R. Metric of a Rotating, Charged Mass. *Commun. in Math. Phys.* **1965**, *6*, 918–919.
- [4] Carter, B. Global Structure of the Kerr Family of Gravitational Fields. *Phys. Rev.* **1968**, *174*, 1559–1571.
- [5] Misner, C.W.; Thorne, K.S.; Wheeler J.A. *Gravitation*; W. H. Freeman: San Francisco, CA, USA, 1973.
- [6] Chandrasekhar, S. The Mathematical Theory of Black Holes. In *The International Series of Monograph on Physics*; Clarendon Press: Oxford, UK, 1983; Ch. 7, Volume 69.
- [7] Tchekhovskoy, A.; Narayan, R.; McKinney, J.C. Efficient generation of jets from magnetically arrested accretion on a rapidly spinning black hole. *Mon. Not. R. Astron. Soc.* **2011**, *418*, L79–L83.
- [8] Tchekhovskoy, A.; McKinney, J.C.; Narayan, R. General Relativistic Modeling of Magnetized Jets from accretion Black Holes. *Journal of Physics Conference Series* **2012**, *372*, 012040.
- [9] McKinney, J.C.; Tchekhovskoy A.; Blandford R.D. General relativistic magnetohydrodynamic simulations of magnetically choked accretion flows around black holes. *Mon. Not. R. Astr. Soc.* **2012**, *423*, 3083–3117.
- [10] Ressler, S.M.; Tchekhovskoy, A.; Quataert, E.; Chandra, M.; Gammie, C.F. Electron thermodynamics in GRMHD simulations of low-luminosity black hole accretion. *Mon. Not. R. Astr. Soc.* **2015**, *454*, 1848–1870.
- [11] Ressler, S.M.; Tchekhovskoy, A.; Quataert, E.; Gammie, C.F. The disc-jet symbiosis emerges: modelling the emission of Sagittarius A* with electron thermodynamics. *Mon. Not. R. Astr. Soc.* **2017**, *467*, 3604–3619.
- [12] Foucart, F.; Chandra, M.; Gammie, C.F.; Quataert, E.; Tchekhovskoy, A. How important is non-ideal physics in simulations of sub-Eddington accretion on to spinning black holes? *Mon. Not. R. Astr. Soc.* **2017**, *470*, 2240–2252.
- [13] Ryan, B.R.; Ressler, S.M.; Dolence, J.C.; Gammie, C.F.; Quataert, E. Two-Temperature GRRMHD Simulations of M87. *Astrophys. J.* **2018**, *864*, 126, 13 pp.
- [14] Blandford, R.D.; Znajek, R.L. Electromagnetic extraction of energy from Kerr black holes. *MNRAS* **1977**, *179*, 433.
- [15] Dokuchaev, V.I.; Nazarova, N.O. Event horizon image within black hole shadow. *J. Exp. Theor. Phys.* **2019**, *128*, 578–585.
- [16] Dokuchaev, V.I.; Nazarova, N.O. Silhouettes of invisible black holes. *Phys. Usp.* **2020**, *63*, 583–600.
- [17] Bardeen, J.M. *Black Holes*; DeWitt, C., DeWitt, B. S., Eds.; Gordon and Breach Science Publishers: New York, NY, USA, 1973; pp. 215–239.
- [18] Bisnovaty-Kogan, G.S.; Tsupko O.Yu. Shadow of a black hole at cosmological distances. *Phys. Rev. D* **2018**, *98*, 084020.
- [19] Cunningham, C.T.; Bardeen, J.M. The Optical Appearance of a Star Orbiting an Extreme Kerr Black Hole. *Astrophys. J.* **1972**, *173*, L137–L142.
- [20] Cunningham, C.T.; Bardeen, J.M. The Optical Appearance of a Star Orbiting an Extreme Kerr Black Hole. *Astrophys. J.* **1973**, *183*, 237–264.
- [21] The Event Horizon Telescope Collaboration: First M87 Event Horizon Telescope Results. I. The Shadow of the Supermassive Black Hole. *Astrophys. J.* **2019**, *875*, L1.
- [22] The Event Horizon Telescope Collaboration: First M87 Event Horizon Telescope Results. II. Array and Instrumentation. *Astrophys. J.* **2019**, *875*, L2.
- [23] The Event Horizon Telescope Collaboration: First M87 Event First M87 Event Horizon Telescope Results. III. Data Processing and Calibration. *Astrophys. J.* **2019**, *875*, L3.
- [24] The Event Horizon Telescope Collaboration: First M87 Event First M87 Event Horizon Telescope Results. IV. Imaging the Central Supermassive Black Hole. *Astrophys. J.* **2019**, *875*, L4.
- [25] The Event Horizon Telescope Collaboration: First M87 Event First M87 Event Horizon Telescope Results. V. Physical Origin of the Asymmetric Ring. *Astrophys. J.* **2019**, *875*, L5.
- [26] The Event Horizon Telescope Collaboration: First M87 Event First First M87 Event Horizon Telescope Results. VI. The Shadow and Mass of the Central Black Hole. *Astrophys. J.* **2019**, *875*, L6.
- [27] Event Horizon Telescope Collaboration. First Sagittarius A* Event Horizon Telescope Results. I. The Shadow of the Supermassive Black Hole in the Center of the Milky Way. *Astrophys. J.* **2022**, *930*, L12.
- [28] Dokuchaev, V.I. Spin and mass of the nearest supermassive black hole. *Gen. Relativ. Gravit.* **2014**, *46*, 1832–1845.
- [29] Dokuchaev, V.I. To see invisible: image of the event horizon within the black hole shadow. *Int. J. Mod. Phys. D* **2019**, *28*, 1941005.
- [30] Dokuchaev, V. I.; Nazarova, N. O. The Brightest Point in Accretion Disk and Black Hole Spin: Implication to the Image of Black Hole M87*. *Universe* **2019**, *5*, 183.
- [31] Dokuchaev, V.I. Physical origin of the dark spot at the image of supermassive black hole SgrA* revealed by the EHT collaboration. *Astronomy* **2022**, *1(2)*, 93–98.
- [32] Reynolds, C.S. Observing black holes spin. *Nature Astronomy* **2019**, *3*, 41–47.
- [33] Nokhrina, E.E.; Gurvits, L.I.; Beskin, V.S.; Nakamura, M.; Asada, K.; Hada, K. M87 black hole mass and spin estimate through the position of the jet boundary shape break. *MNRAS* **2019**, *489*, 1197–1205.
- [34] Ayzenberg, D.; et al. Fundamental Physics Opportunities with the Next-Generation Event Horizon Telescope. **2023**; arXiv:2312.02130 [astro-ph.HE].
- [35] Dokuchaev, V.I.; Nazarova, N.O. Gravitational lensing of a star by rotating black hole, *JETP Letters* **2017**, *106*, 637–642.
- [36] Dokuchaev, V.I.; Nazarova, N.O. Star motion around rotating black hole. **2018**; <https://youtu.be/P6DneV0vk7U>.
- [37] Dokuchaev, V.I.; Nazarova, N.O. Infall of the star into rotating black hole viewed by a distant observer. **2018**; <https://youtu.be/fps-3frL0AM>.
- [38] Dokuchaev, V.I.; Nazarova, N.O. Modeling the motion of a bright spot in jets from black holes M87* and SgrA*. *Gen. Relativ. Gravit.* **2021**, *53*, 83.

- [39] Dokuchaev, V.I.; Nazarova, N.O.; Smirnov, V.P. Event horizon silhouette: Implications to supermassive black holes M87* and SgrA*. *Gen. Relativ. Gravit.* **2019**, *51*, 81.
- [40] Kardashev, N.S.; Novikov, I. D.; Lukash, V.N.; Pilipenko, S.V.; Mikheeva, E.V.; Bisikalo, D.V.; Wiebe, D.S.; Doroshkevich, A.G.; Zasov, A.V.; Zinchenko, I.I. Review of scientific topics for the Millimetron space observatory. *Phys. Usp.* **2014**, *57*, 1199–1228.
- [41] Rudnitskiy A.G.; Mzhelskiy, P.V.; Shchurov, M.A.; Syachina, T.A.; Zapevalin, P.R. Analysis of Orbital Configurations for Millimetron Space Observatory. *Acta Astronautica* **2022** *196*, 29–41.
- [42] Likhachev, S.F.; Rudnitskiy, A.G.; Shchurov, M.A.; Andrianov, A.S.; Baryshev, A.M.; Chernov, S.V.; Kostenko, V.I. High Resolution Imaging of a Black Hole Shadow with Millimetron Orbit around Lagrange Point L2. *MNRAS* **2022** *511*, 668–682.
- [43] Ivanov, P.B.; et al. Interferometric observations of supermassive black holes in the millimeter wave band. *Phys. Usp.* **2019** *62*, 423–449.